

## Article

# Hierarchical CoNiO<sub>2</sub> Microflowers Assembled by Mesoporous Nanosheets as Efficient Electrocatalysts for Hydrogen Evolution Reaction

Dingfu Zhang<sup>1</sup>, Jiaxin Yao<sup>1</sup>, Jinling Yin<sup>1</sup>, Guiling Wang<sup>1</sup>, Kai Zhu<sup>1,\*</sup> , Jun Yan<sup>1</sup>, Dianxue Cao<sup>1</sup> and Min Zhu<sup>2,\*</sup>

<sup>1</sup> Key Laboratory of Superlight Materials and Surface Technology of Ministry of Education, College of Materials Science and Chemical Engineering, Harbin Engineering University, Harbin 150001, China

<sup>2</sup> Technology Innovation Center of Industrial Hemp for State Market Regulation, College of Chemistry and Chemical Engineering, Qiqihar University, Qiqihar 161006, China

\* Correspondence: kzhu@hrbeu.edu.cn (K.Z.); 03637@qqhru.edu.cn (M.Z.)

**Abstract:** In order to alleviate the energy crisis and propel a low-carbon economy, hydrogen (H<sub>2</sub>) plays an important role as a renewable cleaning resource. To break the hydrogen evolution reaction (HER) bottleneck, we need high-efficiency electrocatalysts. Based on the synergistic effect between bimetallic oxides, hierarchical mesoporous CoNiO<sub>2</sub> nanosheets can be fabricated. Combining physical representations with electrochemical measurements, the resultant CoNiO<sub>2</sub> catalysts present the hierarchical microflowers morphology assembled by mesoporous nanosheets. The ultrathin two-dimensional nanosheets and porous surface characteristics provide the vast channels for electrolyte injection, thus endowing CoNiO<sub>2</sub> the outstanding HER performance. The excellent performance with a fewer onset potential of 94 mV, a smaller overpotential at 10 mA cm<sup>-2</sup>, a lower Tafel slope of 109 mV dec<sup>-1</sup> and better stability after 1000 cycles makes CoNiO<sub>2</sub> better than that of metallic Co and metallic Ni.

**Keywords:** hydrogen evolution reaction; synergistic effect; CoNiO<sub>2</sub> nanosheets; electrocatalysis



**Citation:** Zhang, D.; Yao, J.; Yin, J.; Wang, G.; Zhu, K.; Yan, J.; Cao, D.; Zhu, M. Hierarchical CoNiO<sub>2</sub> Microflowers Assembled by Mesoporous Nanosheets as Efficient Electrocatalysts for Hydrogen Evolution Reaction. *Materials* **2023**, *16*, 2204. <https://doi.org/10.3390/ma16062204>

Academic Editors: Yuhang Ren and Jun Ouyang

Received: 15 February 2023

Revised: 2 March 2023

Accepted: 7 March 2023

Published: 9 March 2023



**Copyright:** © 2023 by the authors. Licensee MDPI, Basel, Switzerland. This article is an open access article distributed under the terms and conditions of the Creative Commons Attribution (CC BY) license (<https://creativecommons.org/licenses/by/4.0/>).

## 1. Introduction

Fossil fuels are running out and the planet is getting worse, meaning it is really important to develop high-power and energy density alternative energy devices. There is no doubt that hydrogen (H<sub>2</sub>) is a renewable and clean energy that can be obtained from the environment [1–4]. It is well known that hydrogen is the most abundant element on earth; currently, 90% of H<sub>2</sub> is acquired from fossil fuels, leading to the aggravation of the energy crisis [5]. Electrocatalytic water (H<sub>2</sub>O) splitting, using H<sub>2</sub>O as the hydrogen source and powered by renewable electricity, is regarded as a potential H<sub>2</sub> synthesis strategy to minimize carbon emissions [6–10]. The hydrogen evolution reaction (HER) is, however, still limited by the large overpotential that is found in splitting H<sub>2</sub>O, which makes the reaction performance hover at a significantly lower level. It has been shown that certain noble metals with the low overpotential, such as platinum-based materials, are expected to serve as excellent catalysts for hydrogen production in practical application, though the scarcity of these materials and the high price make them difficult to use in practice [11–14]. To solve HER problems, we need efficient non-precious metal electrocatalysts [15–20].

To date, non-precious metals as the substitute materials have been extensively explored for HER to replace precious metals. By virtue of their structure design and synergistic effect, catalysts are capable of introducing hydrogen into a system at a higher performance level. There is a possibility of increasing the electrochemical HER performance by increasing the number of active sites in nanosheet structures. For example, Ni<sub>0.85</sub>Se nanosheet on graphene owns many active sites and well HER catalytic property [21]. It may also be advantageous to improve performance by taking advantage of the synergistic effects of

bimetallic electrocatalysts. Singh et al. reported that the B-TiZr-2.5 catalyst has improved HER activity [22]. It is recognized that the single metal catalyst is not enough to make the HER catalyst active. Therefore, other metal oxide phases need to be added to obtain higher HER performance.

It is well known that most transition monometal oxides have a very good catalytic activity, but due to their low active site and specific surface area, their further applications are limited. Due to this, many efforts have been made in order to further enhance the catalytic properties of transition monometal oxides. Among them, the introduction of bimetallic oxides is a strategy. Wang et al. reported that  $\text{NiCo}_2\text{O}_4 @ \text{Ni}(\text{OH})_2/\text{NiOOH}$  catalyst has the improved HER activity [23]. In view of the synergistic effect, developing the efficient Co-Ni oxide catalysts by a simple and cost-effective method is attractive and necessary for HER [24]. Herein, hierarchical  $\text{CoNiO}_2$  microflowers assembled by mesoporous nanosheets are synthesized successfully by a simple hydrothermal method together with an annealing process. Benefitting from the large specific surface area and synergistic effect between Ni-Co metals, this resultant  $\text{CoNiO}_2$  shows stunning catalytic properties for HER, such as the low Tafel slope of  $109 \text{ mV dec}^{-1}$ , small onset potential of 94 mV, low charge transfer resistance and a long-term stable behavior regarding catalysis.

## 2. Experimental

### 2.1. Synthesis of $\text{CoNiO}_2$

The hierarchical  $\text{CoNiO}_2$  microflower was prepared [25,26]; concretely, an ethanol-water (2:1 *v/v*) mixture containing 0.73 g  $\text{Ni}(\text{NO}_3)_2 \cdot 6\text{H}_2\text{O}$ , 1.45 g  $\text{Co}(\text{NO}_3)_2 \cdot 6\text{H}_2\text{O}$  and 1.4 g hexamethylenetetramine (HMT). This was then transferred into a 50 mL autoclave lined with Teflon after it had been stirred for 30 min. Upon sealing the autoclave, it was placed into an electric oven which had been set at  $95^\circ\text{C}$  for 8 h. We first cooled down the as-obtained Co-Ni precursors under a vacuum to room temperature, washed with water and ethanol several times to remove the unreacted residues, followed by drying at  $60^\circ\text{C}$  for 8 h under vacuum to ensure the precursors were completely dry. Lastly,  $\text{CoNiO}_2$  was synthesized following annealing at 450 degrees Celsius in an Ar atmosphere for two hours at  $1^\circ\text{C}$  per minute. For comparison, the individual Ni and Co catalysts were procured by the same method without adding Cobaltous nitrate hexahydrate and Nickel nitrate hexahydrate, respectively.

### 2.2. Characterizations

In terms of surface analysis, X-ray Photoelectron Spectroscopy (XPS, ESCALAB250) is a practical method that can be used for both qualitative and quantitative analyses of solid surfaces, as well as structural identification. X-ray diffraction (XRD, Rigaku TTR III) is a research method to obtain information such as the composition of materials, the structure or morphology of molecules in materials. Scanning electron microscope (FESEM, FEI Quanta 200 FEG) can not only observe the surface morphology, but also analyze the components and elements. Transmission Electron Microscopy (TEM) and High-Resolution TEM (HRTEM) are instruments for imaging and analyzing the microstructure of materials (FEI Tecnai G2 F20).

### 2.3. Electrochemical Measurements

It took 550  $\mu\text{L}$  of 6/5 (*v/v*) water/ethanol solution, 5 mg of  $\text{CoNiO}_2$  powder and 20  $\mu\text{L}$  of Nafion (5 wt %) to make the mixed solution and this was sonicated mildly for 30 min. Then, 5  $\mu\text{L}$  of the prepared catalyst solution was evenly coated on carbon fiber cloth with an area of  $1 \text{ cm}^2$ . Typical electrochemical measurements were carried out using a three-electrode setup involving the working electrode (the loaded carbon cloth), as well as the reference electrode (the Hg/HgO solution) and the counter electrode (the carbon rod). According to the equation below, the potentials reported in this study have been converted to the reversible hydrogen electrode (RHE) scale and are now expressed as follows:

$E(\text{RHE}) = E(\text{Hg}/\text{HgO}) + 0.098 + 0.0592 \times \text{pH}$ . The electrocatalytic experiments were carried out on an Autolab PGSTAT 302 (Eco Chemie) workstation.

### 3. Results and Discussion

The synthetic method can be demonstrated visually in Figure 1, in which a two-step method had been used to prepare the typical mesoporous  $\text{CoNiO}_2$ . Hydrothermal processes are characterized by the hydrolysis of ethanol and hexamethylenetetramine, forming carbonate ion and hydroxide ion, which are then reacted with  $\text{Ni}^{2+}$  and  $\text{Co}^{2+}$  to form precursors of nickel and cobalt hydroxy-carbonates during the reaction. Secondly, under the Ar atmosphere, the as-prepared Ni-Co precursor was transformed into mesoporous  $\text{CoNiO}_2$  with a hierarchical structure. Furthermore, individual Co and Ni catalysts were prepared so that the synergistic effect of these components could be evaluated.

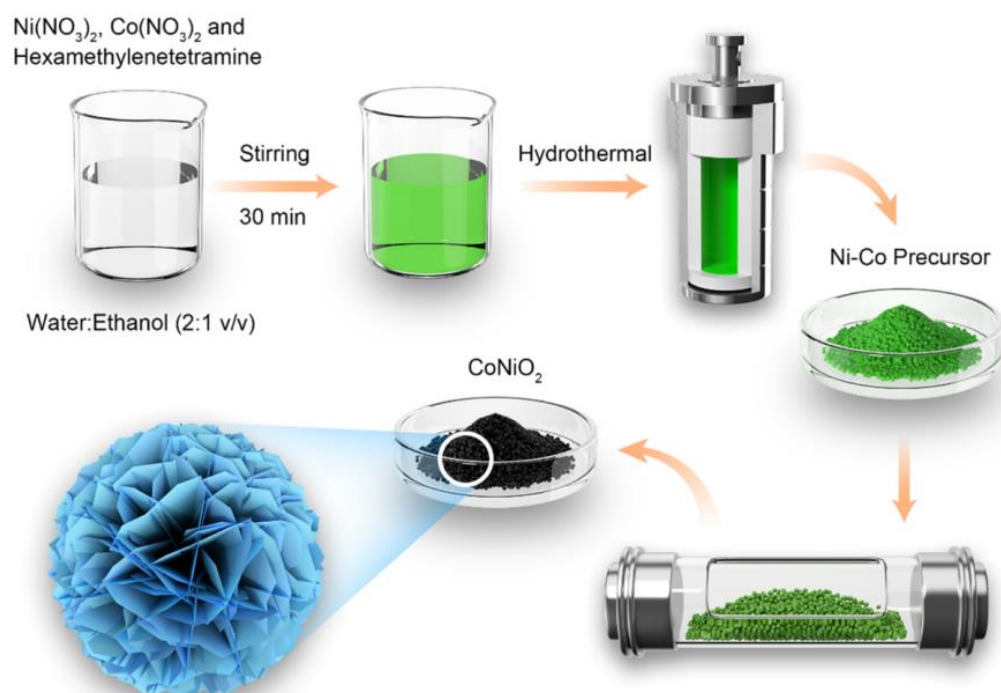


**Figure 1.** The fabrication procedure is illustrated in this schematic diagram for hierarchical  $\text{CoNiO}_2$  microflowers assembled by mesoporous nanosheets.

To investigate the crystal structure of the electrocatalyst, an XRD analysis has been carried out. The characteristic peaks of  $\text{CoNiO}_2$  in Figure 2 located at  $36.8^\circ$ ,  $42.8^\circ$  and  $61.8^\circ$  correspond to the (111), (200) and (220) planes of the cubic  $\text{CoNiO}_2$  (JCPDS No. 10-0188) [25,26]. Meanwhile, the (111), (200) and (220) planes of metallic Ni can be matched to the diffraction peaks of Ni specimens at  $44.5^\circ$ ,  $51.8^\circ$  and  $76.4^\circ$  (JCPDS No.04-0850) [27]. The characteristic peaks of the Co sample located at  $41.7^\circ$ ,  $44.7^\circ$ ,  $47.6^\circ$  and  $75.9^\circ$  are associated to the (100), (002), (101) and (110) of the metallic Cobalt's planes (JCPDS No. 05-0727) [28]. It was observed that there were no significant peaks of impurities, which indicated that the products were phase pure. Particularly, compared with the single metallic Ni or Co specimen,  $\text{CoNiO}_2$  presents the weaker peak intensities. The relatively poor crystallinity means that  $\text{CoNiO}_2$  exhibits the thinner thickness and higher defects concentration, which is expected to show better activity in the hydrogen evolution reaction.

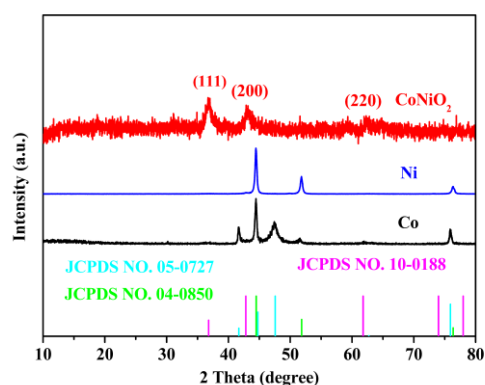


**Figure 2.** An XRD pattern showing the crystalline structure of  $\text{CoNiO}_2$ , Ni and Co.

Electrocatalysts were characterized morphologically using scanning electron microscopy (SEM). As shown in the low-magnification SEM image (Figure 3a,b), the as-prepared  $\text{CoNiO}_2$  material presents the flower-like microsphere structure with an average diameter of about  $9\ \mu\text{m}$ . According to the high-resolution SEM images, it is also evident that the microflowers are a result of the two-dimensional thin nanosheets that are assembled into the microflowers (Figure 3c,d). For comparison, the morphologies of the metallic Ni and metallic Co were also provided, as shown in Figure 3e,f. It is worth noting that the individual Ni and Co samples are formed by spherical particles along with the severe agglomeration simultaneously. Having a regular and open hierarchical structure gives  $\text{CoNiO}_2$  a more specific surface area, makes electrolyte injection efficient and helps it be more catalytic. The conductivity of  $\text{CoNiO}_2$  material obtained after calcination is increased, which makes hydrogen evolution easier. The above results show that the prepared  $\text{CoNiO}_2$  material has a large specific surface area, exposed more active sites and good conductivity. Figure 3g–j shows the SEM picture and the elemental mapping pictures for  $\text{CoNiO}_2$  materials, indicating the good distribution of Ni, Co and O elements in the hierarchical flower-like nanosheets.

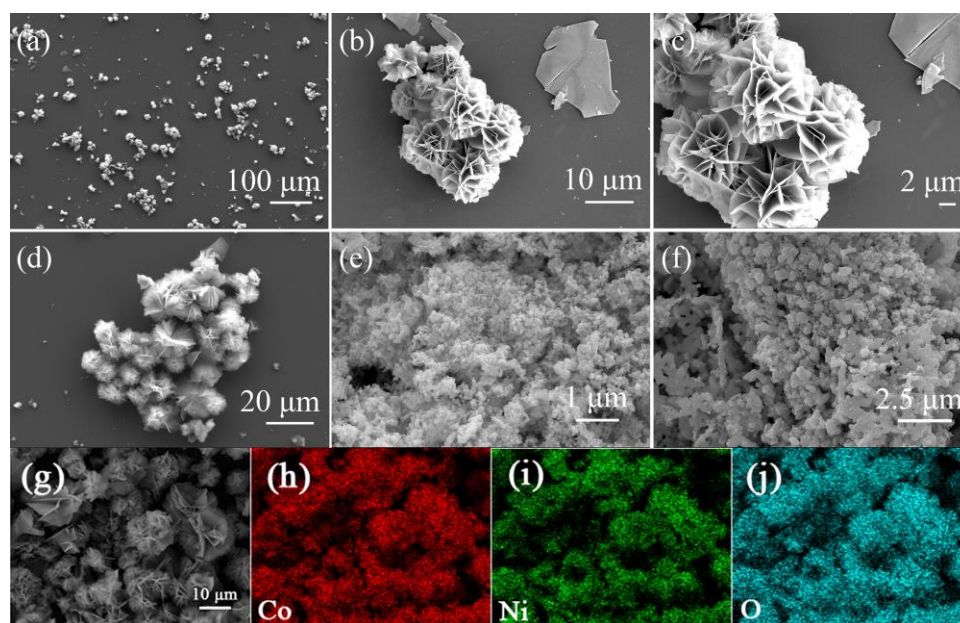


**Figure 3.** SEM images of (a–d) the hierarchical  $\text{CoNiO}_2$ , (e) the metallic Ni and (f) the metallic Co. SEM picture of (g)  $\text{CoNiO}_2$  and (h–j) the homologous elemental mapping pictures of Co, Ni and O for  $\text{CoNiO}_2$  materials.

We investigated the morphology of the as-prepared  $\text{CoNiO}_2$  sample by transmission electron microscopy and high-resolution transmission electron microscopy in a further study. According to the TEM images of  $\text{CoNiO}_2$  shown in Figure 4a–d, the thin nanosheets are used to construct the microflowers, and therefore, TEM images are in agreement with SEM observations, where the nanosheets are assembled by thin walls. A distinctive characteristic of  $\text{CoNiO}_2$  microflowers is that they are formed by thin nanosheets of  $\text{CoNiO}_2$  over a thickness of approximately 100–300 nanometers. In Figure 4e, it is depicted that the lattice fringes with separations of 0.211 nanometers and 0.244 nanometers correspond to the crystallographic planes (200) and (111) for cubic  $\text{CoNiO}_2$ , respectively. It is also worth mentioning that the SAED image exhibits a pattern along the zone axis of the [110] zone of cubic  $\text{CoNiO}_2$ , which further confirms that  $\text{CoNiO}_2$  phase has been successfully generated (Figure 4f).

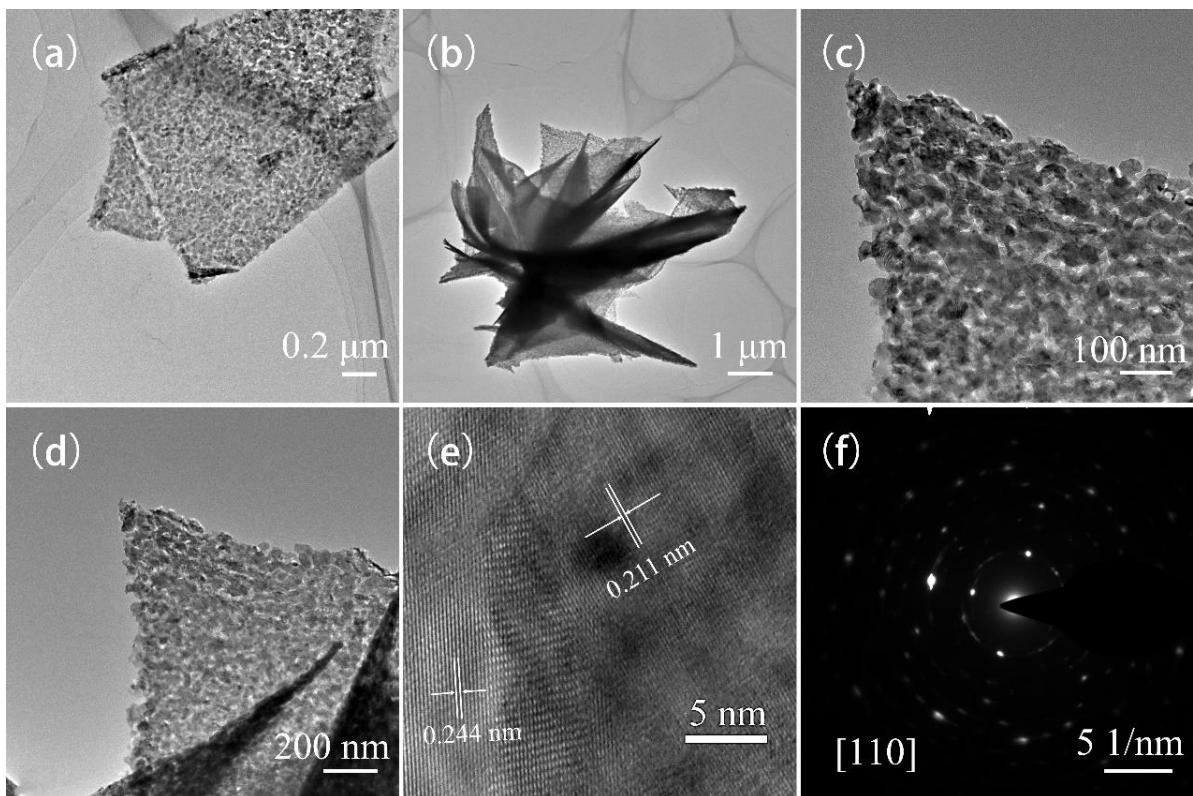


**Figure 4.** (a–d) TEM figures, (e) HRTEM figure and (f) SAED pattern of  $\text{CoNiO}_2$ .

Further confirmations of surface elemental composition were done using X-ray photoelectron spectroscopy (Figure 5). Figure 5a shows the full scan spectrum of  $\text{CoNiO}_2$ , in which Co, Ni and O elements coexist. According to the Co 2p spectra (Figure 5b), the binding energies at 795.0 eV and 779.8 eV correspond to the peaks of Co 2p<sub>1/2</sub> and Co 2p<sub>3/2</sub>, respectively, while the satellite peaks of 803.3 eV and 785.9 eV are associated with its satellites [29]. A correlation was found between Ni 2p<sub>3/2</sub> and Ni 2p<sub>1/2</sub>, as indicated by the characteristic peaks of Ni 2p in Figure 5c located at 854.0 eV and 872.8 eV, and the relevant satellite peaks were also observed at 861.1 eV and 879.5 eV [30]. There are also two characteristic peaks in the O 1s spectrum (Figure 5d); one at 529.6 eV represents oxygen species in the  $\text{CoNiO}_2$  phase and the other represents oxygen-containing residuals like H-O-H. Based on the above characterizations, the hierarchical  $\text{CoNiO}_2$  microspheres are synthesized successfully.

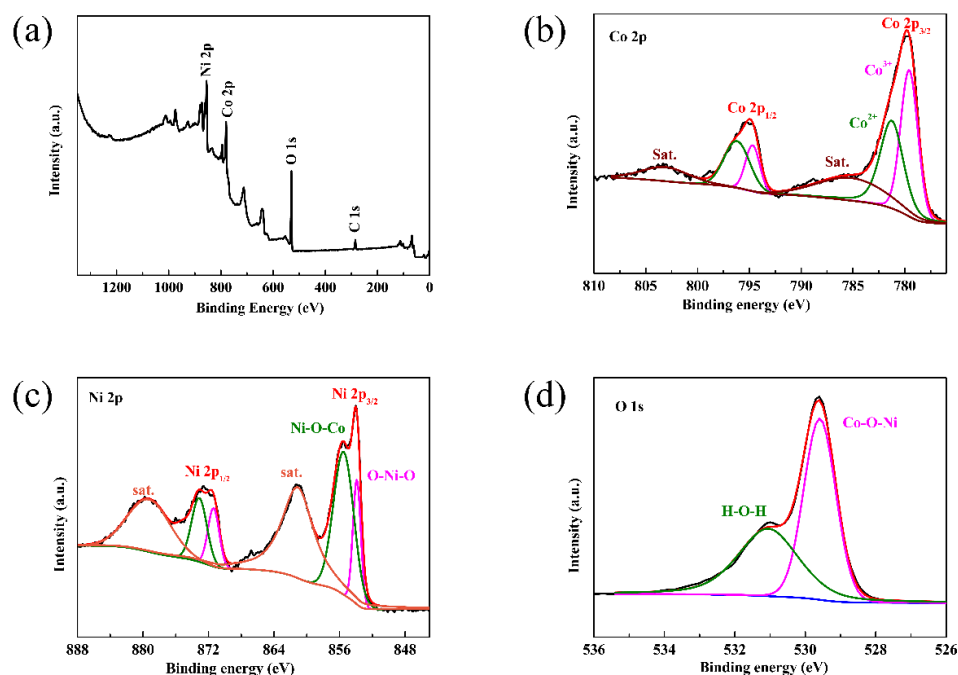


**Figure 5.** (a) Survey spectrum, (b) Co 2p, (c) Ni 2p and (d) O 1s for CoNiO<sub>2</sub> of XPS spectra.

Using a typical three-electrode setup that contained a concentration of 1 M KOH, hierarchical CoNiO<sub>2</sub>, metallic Ni and metallic Co were investigated for their electrocatalytic activities. Figure 6a illustrates that HER polarization curves were measured at 1 mV s<sup>-1</sup> with IR correction for CoNiO<sub>2</sub>, Ni, Co and bare carbon cloth. The CoNiO<sub>2</sub> catalyst has a lower onset overpotential of 94 mV when compared to Ni and Co catalysts, and has a faster current response when the potential goes up, while pure carbon cloth has negligible electrocatalytic activity. Furthermore, CoNiO<sub>2</sub> has only an overpotential of 170 mV at 10 mA cm<sup>-2</sup>, which is lower than that of Ni (188 mV) and Co (244 mV), showing that it has a superior catalytic activity compared to these two metals. The HER performance of CoNiO<sub>2</sub> is also superior to other Co-Ni composite materials reported previously (Table 1), which benefits from the nanoflower structure providing more active sites and the synergistic effect.

**Table 1.** In 1 M KOH, CoNiO<sub>2</sub> electrocatalyst performance in HER was compared with that of cobalt- and nickel-based electrocatalysts.

Catalyst	Current Density (mA·cm <sup>-2</sup> )	Potential (mV)	Reference
NiFe-LDH/NiCo <sub>2</sub> O <sub>4</sub>	10	192	[31]
NiCo <sub>2</sub> O <sub>4</sub> nanowires	10	294	[31]
Ni/NiO	10	226	[32]
Air- NiCo <sub>2</sub> O <sub>4</sub>	10	226	[33]
Ni@NiO	10	192	[34]
Ni <sub>3</sub> S <sub>2</sub> @Ni(OH) <sub>2</sub>	10	237	[35]
CeO <sub>2</sub> /Co(OH) <sub>2</sub>	10	317	[36]
CoO-3D graphene	10	360	[37]
Co-Ni hybrid oxides	10	378	[38]
MoS <sub>x</sub> @NiO	10	406	[39]
CoNiO <sub>2</sub>	10	170	This work

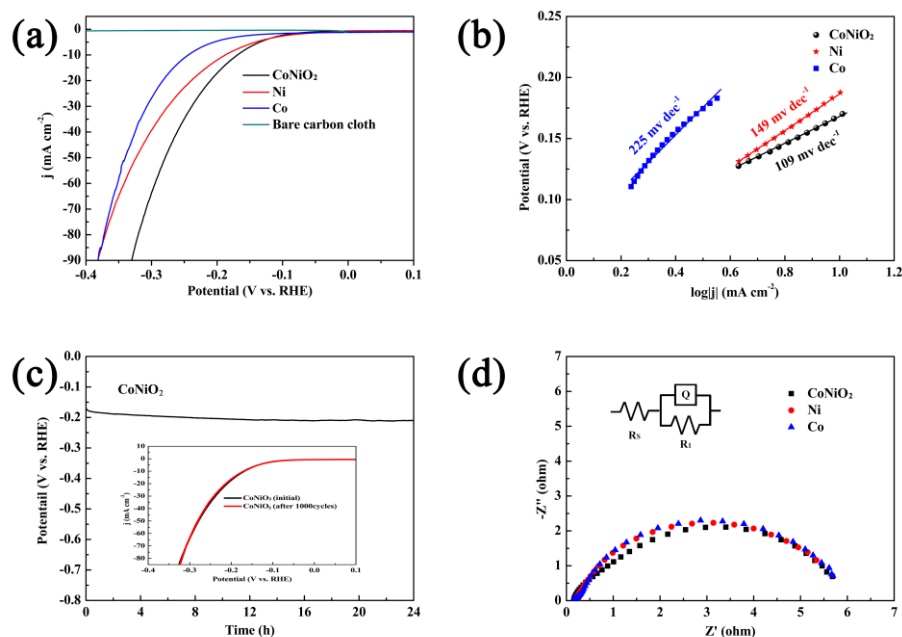


**Figure 6.** (a) Polarization curves and the corresponding (b) slopes of Tafel of CoNiO<sub>2</sub>, metallic Ni and metallic Co, respectively. (c) Chronopotentiometry curve of CoNiO<sub>2</sub> at 10 milliampere square centimeter for 24 h. This inset shows the polarization curves of the material before and after a 1000 cycles period. (d) Nyquist plots of the CoNiO<sub>2</sub>, metallic Ni and metallic Co at  $-300$  mV overpotential.

We further explored the inherent properties of different catalysts by evaluating the reaction kinetics of HER using Tafel plots as a way. Figure 6b illustrates that the Tafel slope of CoNiO<sub>2</sub> is  $109 \text{ mV dec}^{-1}$ , a value lower than both Ni ( $149 \text{ mV dec}^{-1}$ ) and Co catalysts ( $225 \text{ mV dec}^{-1}$ ). As indicated by the Tafel slope of  $109 \text{ mV dec}^{-1}$ , the hydrogen evolution process on CoNiO<sub>2</sub> is governed by the Volmer-Heyrovsky mechanism, and the lower value is indicative of the more favorable characteristics of its kinetic behavior toward hydrogen evolution.

The stability and durability of the as-synthesized CoNiO<sub>2</sub> are also evaluated in alkaline condition. Figure 6c shows that the chronopotentiometry curve shows no obvious degradation after 10 h at  $10 \text{ mA cm}^{-2}$ . As can be seen from Figure 6c (inset), the polarization curve starts to overlap the initial curve almost completely, and this maintains the current density of 98.2% even after 1000 continuous sweeping cycles. All the above results prove that CoNiO<sub>2</sub> has excellent HER activity, along with great stability.

Using electrochemical impedance spectroscopy (EIS), we conducted an analysis with an overpotential of  $-300$  mV in order to better understand the HER kinetics of CoNiO<sub>2</sub>, metallic Ni and metallic Co. Figure 6d shows the corresponding Nyquist plots and Figure 6d inset shows the equivalent circuit model. It is clearly observed that CoNiO<sub>2</sub> presents the lowest charge transport resistance ( $R_{ct}$ ), reflecting its better electronic conductivity. Specifically, CoNiO<sub>2</sub>, Ni and Co possess  $R_{ct}$  values of 5.13, 5.27 and 5.35  $\Omega$ , respectively. Smaller  $R_{ct}$  values indicate that CoNiO<sub>2</sub> owns quicker charge transfer than other samples. During the HER process of CoNiO<sub>2</sub>, the electrons deliver directly and efficiently between the catalyst and the solution, contributing well to activity.

An electrochemical surface area with a higher value typically means there are more active sites in the electrochemical layer, which results in higher HER activity. In addition, the electrochemical surface area varies with the capacitance of the double layer, so that it is proportional to the surface area. There are several CV curves that can be seen in Figure 7a–c related to electrocatalysts that have been tested with a scan rate that ranges from 20 to  $100 \text{ mV s}^{-1}$ , namely CoNiO<sub>2</sub>, metallic Ni and metallic Co in an alkaline electrolyte. At 0.77 V, we calculated the current density difference between the anode and cathode ( $\Delta j = J_{\text{anode}} - J_{\text{cathode}}$ ). It can be obtained twice the value of double-layer capacitance

( $C_{dl}$ ) by fitting the scanning rate and  $\Delta j$  together. As you can see in Figure 7d,  $\text{CoNiO}_2$  has a large  $C_{dl}$  value ( $8.05 \times 10^{-4} \text{ mF cm}^{-2}$ ) compared to metallic Ni ( $5.10 \times 10^{-4} \text{ mF cm}^{-2}$ ) and metallic Co ( $3.15 \times 10^{-4} \text{ mF cm}^{-2}$ ). There was a noticeable difference between  $\text{CoNiO}_2$  and all the other materials investigated in respect of their electrochemical surface area and HER activity in the alkaline electrolyte based on the results.

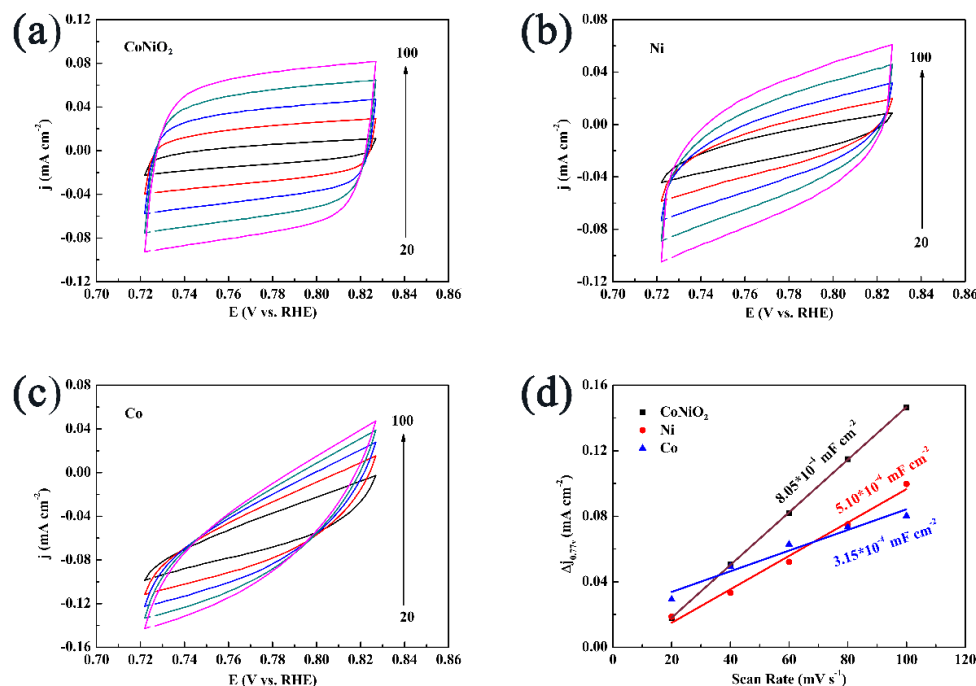


**Figure 7.** The CV curves of (a)  $\text{CoNiO}_2$ , (b) metallic Ni and (c) metallic Co. (d) The double-layer capacitance values  $\text{CoNiO}_2$ , metallic Ni and metallic Co in 1 M KOH.

The composition of the  $\text{CoNiO}_2$  process was examined by XRD following the HER for 10 h. As shown in Figure 8a, the XRD curves before and after 10 h test of  $\text{CoNiO}_2$  in an alkaline electrolyte have been displayed. The results show that all the peaks after the 10 h test have remained approximately the same as they were before the test, which proves that the  $\text{CoNiO}_2$  in an alkaline electrolyte is a very stable compound. SEM images (Figure 8b) were taken of the same samples after 10 h of HER in an alkaline electrolyte, which indicate that the morphologies after the test are nanoparticles agglomerated compared to the ones before the test.

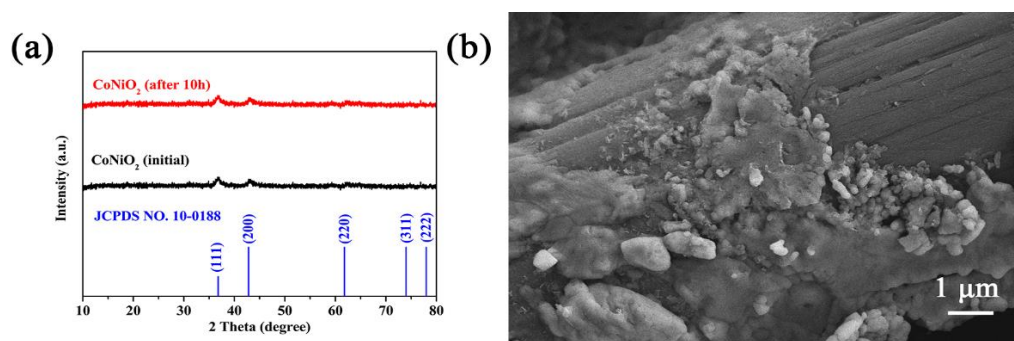


**Figure 8.** (a) XRD patterns of before and after a 10 h test of  $\text{CoNiO}_2$  in an alkaline electrolyte. (b) SEM images of after a 10 h test of  $\text{CoNiO}_2$  in an alkaline electrolyte.

As shown in Figure 9a, the characteristic peak of the cobalt-nickel precursor located at  $9.5^\circ$  corresponds to the (001) planes of  $\text{Co}(\text{OH})_2$  (JCPDS No. 51-1731), and is located at  $19.3^\circ$

(001) planes of  $\text{Ni}(\text{OH})_2$  (JCPDS No. 14-0117). As shown in the SEM image (Figure 9a,b), the cobalt-nickel precursor presents the flower-like microsphere structure.

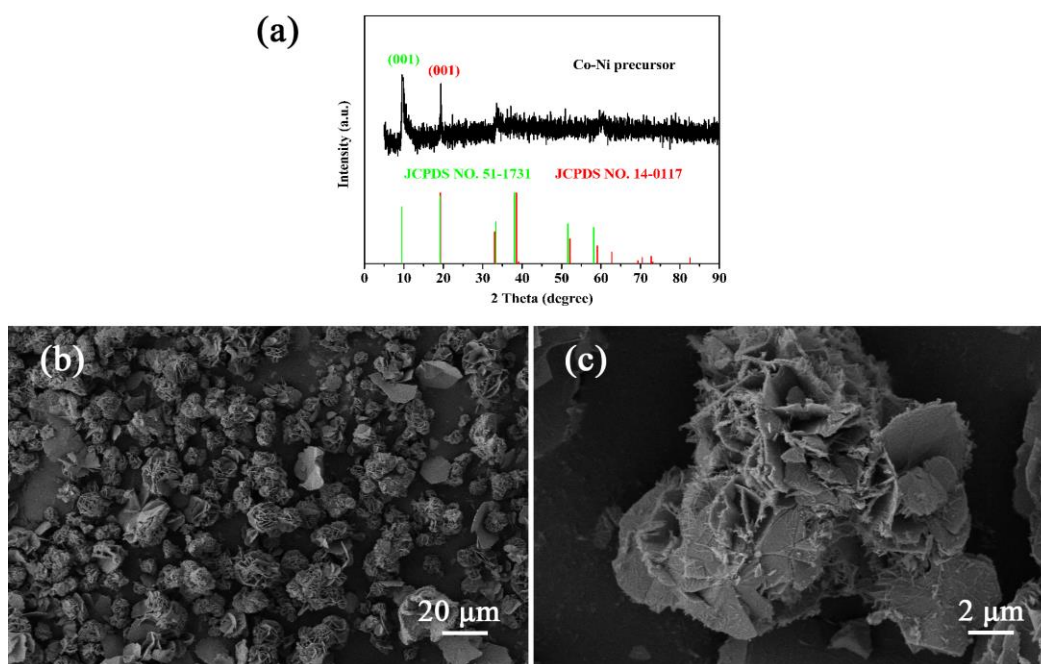


**Figure 9.** (a) XRD patterns of the cobalt-nickel precursor. (b,c) SEM images of the cobalt-nickel precursor.

The surface elemental composition of the  $\text{CoNiO}_2$  process was examined by XPS following the post-HER. As shown in Figure 10, the XPS curves of  $\text{CoNiO}_2$  of the post-HER in an alkaline electrolyte have been displayed. The results show that the chemical surface composition of post-HER is the same as before and that there is no difference, which proves that the  $\text{CoNiO}_2$  in an alkaline electrolyte is a very stable compound.

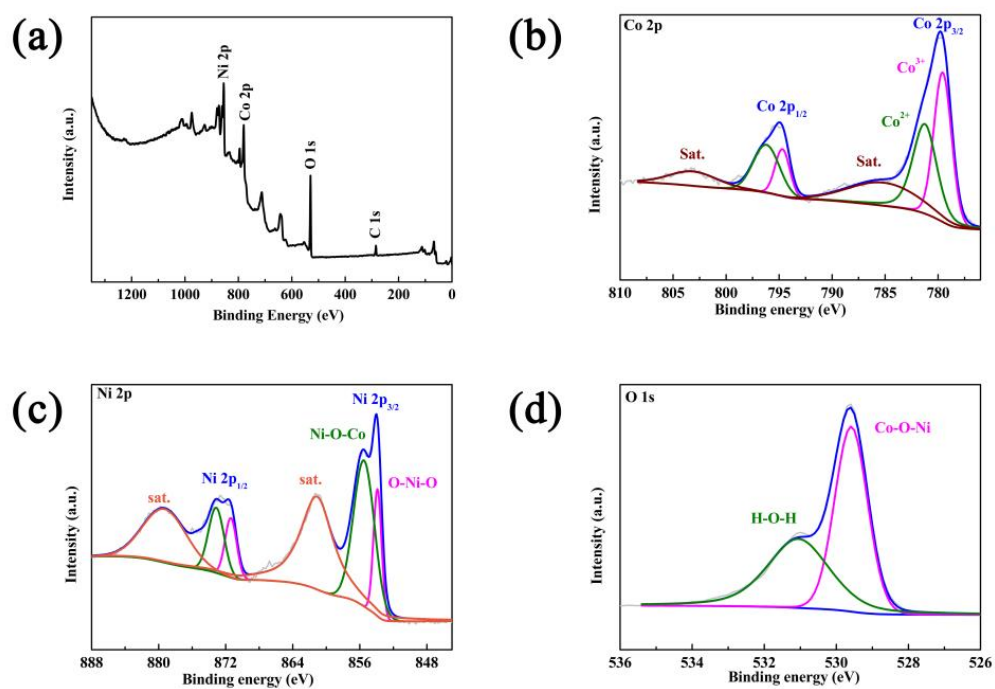


**Figure 10.** (a) Survey spectrum, (b) Co 2p, (c) Ni 2p and (d) O 1s for  $\text{CoNiO}_2$  post-HER of XPS spectra.

#### 4. Conclusions

In summary, it can be concluded that the hierarchical mesoporous CoNiO<sub>2</sub> has been successfully prepared, and that this CoNiO<sub>2</sub> can be used as a catalyst in water to catalyze the HER reaction. In HER, CoNiO<sub>2</sub> only has an onset potential of 94 mV and an overpotential of 170 mV at 10 mA cm<sup>-2</sup> due to the synergistic effect, compared with metallic Co and metallic Ni. Meanwhile, CoNiO<sub>2</sub> presents the improved kinetic characteristics with a Tafel slope (109 mV dec<sup>-1</sup>). The enhanced reaction kinetics of CoNiO<sub>2</sub> can be attributed to the high surface area, and are beneficial for contacting with electrolytes and enhancing the transport of charges. Additionally, CoNiO<sub>2</sub> shows very good long-term stability and can withstand for over 10 h. The excellent electrocatalytic activity with high stability makes CoNiO<sub>2</sub> promising for application in HER.

**Author Contributions:** Methodology, D.Z.; formal analysis and investigation, J.Y. (Jiaxin Yao) and J.Y. (Jinling Yin); writing—original draft preparation, G.W. and K.Z.; writing—review and editing, J.Y. (Jun Yan) and M.Z.; and validation, D.C. All authors have read and agreed to the published version of the manuscript.

**Funding:** The work was supported by a grant from the Fundamental Research Funds for Central Universities (No. 3072021CFT1001) and a grant from the Natural Science Foundation of Heilongjiang Province (No. LH2021B007).

**Informed Consent Statement:** Not applicable for studies not involving humans.

**Data Availability Statement:** Due to privacy, data is not provided at this time.

**Acknowledgments:** We gratefully acknowledge financial support of the Fundamental Research Funds for Central Universities and the Natural Science Foundation of Heilongjiang Province.

**Conflicts of Interest:** Neither the authors nor any of their collaborators declare any competing financial interests.

#### References

- Schlapbach, L.; Züttel, A. Hydrogen-storage materials for mobile applications. *Nature* **2001**, *414*, 353–358. [[CrossRef](#)] [[PubMed](#)]
- Schlapbach, L. Technology: Hydrogen-fuelled vehicles. *Nature* **2009**, *460*, 809–811. [[CrossRef](#)] [[PubMed](#)]
- Yan, Q.; Liu, Z.; Bai, X.; Zhang, X.; Gao, R.; Yuan, W.; Chen, Z.; Li, Z.; Li, Y. In situ formed edge-rich Ni<sub>3</sub>S<sub>2</sub>-NiOOH heterojunctions for oxygen evolution reaction. *J. Electrochem. Soc.* **2022**, *169*, 054532. [[CrossRef](#)]
- Battiatto, S.; Bruno, L.; Pellegrino, A.L.; Terrasi, A.; Mirabella, S. ×Optimized electroless deposition of NiCoP electrocatalysts for enhanced water splitting. *Catal. Today* **2022**, *in press*. [[CrossRef](#)]
- Ledendecker, M.; Mondschein, J.S.; Kasian, O.; Geiger, S.; Gohl, D.; Schalenbach, M.; Zeradjanin, A.; Cherevko, S.; Schaak, R.E.; Mayrhofer, K. Stability and activity of non-noble-metal-based catalysts toward the hydrogen evolution reaction. *Angew Chem. Int. Ed. Engl.* **2017**, *56*, 9767–9771. [[CrossRef](#)]
- Walter, M.G.; Warren, E.L.; McKone, J.R.; Boettcher, S.W.; Mi, Q.; Santori, E.A.; Lewis, N.S. Solar water splitting cells. *Chem. Rev.* **2010**, *110*, 6446–6473. [[CrossRef](#)]
- Deng, J.; Zhang, H.; Zhang, Y.; Luo, P.; Liu, L.; Wang, Y. Striking hierarchical urchin-like peapodded NiCo<sub>2</sub>O<sub>4</sub>@C as advanced bifunctional electrocatalyst for overall water splitting. *J. Power Source* **2017**, *372*, 46–53. [[CrossRef](#)]
- Fang, L.; Jiang, Z.; Xu, H.; Liu, L.; Guan, Y.; Gu, X.; Wang, Y. Crystal-plane engineering of NiCo<sub>2</sub>O<sub>4</sub> electrocatalysts towards efficient overall water splitting. *J. Catal.* **2018**, *357*, 238–246. [[CrossRef](#)]
- Wang, L.Y.; Gu, C.D.; Ge, X.; Zhang, J.L.; Zhu, H.Y.; Tu, J.P. A NiCo<sub>2</sub>O<sub>4</sub> shell on a hollow Ni nanorod array core for water splitting with enhanced electrocatalytic performance. *Chemnanomat* **2018**, *4*, 124–131. [[CrossRef](#)]
- Chhetri, K.; Muthurasu, A.; Dahal, B.; Kim, T.; Mukhiya, T.; Chae, S.H.; Ko, T.H.; Choi, Y.C.; Kim, H.Y. Engineering the abundant heterointerfaces of integrated bimetallic sulfide-coupled 2D MOF-derived mesoporous CoS<sub>2</sub> nanoarray hybrids for electrocatalytic water splitting. *Mater. Today Nano* **2022**, *17*, 100146. [[CrossRef](#)]
- Liu, Q.; Wang, E.; Sun, G. Layered transition-metal hydroxides for alkaline hydrogen evolution reaction. *Chin. J. Catal.* **2020**, *41*, 574–591. [[CrossRef](#)]
- Hu, C.; Lv, C.; Liu, S.; Shi, Y.; Song, J.; Zhang, Z.; Cai, J.; Watanabe, A. Nickel phosphide electrocatalysts for hydrogen evolution reaction. *Catalysts* **2020**, *10*, 88. [[CrossRef](#)]
- Wei, Y.; Soomro, R.A.; Xie, X.; Xu, B. Design of efficient electrocatalysts for hydrogen evolution reaction based on 2D MXenes. *J. Energy Chem.* **2021**, *55*, 244–255. [[CrossRef](#)]

14. Shahroudi, A.; Esfandiari, M.; Habibzadeh, S. Nickel sulfide and phosphide electrocatalysts for hydrogen evolution reaction: Challenges and future perspectives. *RSC Adv.* **2022**, *12*, 29440–29468. [[CrossRef](#)] [[PubMed](#)]
15. Anantharaj, S.; Kundu, S.; Noda, S. Progress in nickel chalcogenide electrocatalyzed hydrogen evolution reaction. *J. Mater. Chem. A* **2020**, *8*, 4174–4192. [[CrossRef](#)]
16. Ge, Z.; Fu, B.; Zhao, J.; Li, X.; Ma, B.; Chen, Y. A review of the electrocatalysts on hydrogen evolution reaction with an emphasis on Fe, Co and Ni-based phosphides. *J. Mater. Sci.* **2020**, *55*, 14081–14104. [[CrossRef](#)]
17. Bai, S.; Yang, M.; Jiang, J.; He, X.; Zou, J.; Xiong, Z.; Liao, G.; Liu, S. Recent advances of MXenes as electrocatalysts for hydrogen evolution reaction. *NPJ 2D Mater. Appl.* **2021**, *5*, 78. [[CrossRef](#)]
18. Kandel, M.R.; Pan, U.N.; Paudel, D.R.; Dhakal, P.P.; Kim, N.H.; Lee, J.H. Hybridized bimetallic phosphides of Ni–Mo, Co–Mo, and Co–Ni in a single ultrathin-3D-nanosheets for efficient HER and OER in alkaline media. *Compos. Part B Eng.* **2022**, *239*, 109992. [[CrossRef](#)]
19. Battiato, S.; Pellegrino, A.L.; Pollicino, A.; Terrasi, A.; Mirabella, S. Composition-controlled chemical bath deposition of Fe-doped NiO microflowers for boosting oxygen evolution reaction. *Int. J. Hydrogen Energy* **2023**, *in press*. [[CrossRef](#)]
20. Kim, J.; Jang, Y.J.; Jang, Y.H. Electrodeposition of Stable Noble-Metal-Free Co-P Electrocatalysts for Hydrogen Evolution Reaction. *Materials* **2023**, *16*, 593. [[CrossRef](#)]
21. Zhu, M.; Yan, Y.D.; Yan, Q.; Yin, J.L.; Cheng, K.; Ye, K.; Zhu, K.; Yan, J.; Cao, D.X.; Wang, G.L. In situ growth of Ni<sub>0.85</sub>Se on graphene as a robust electrocatalyst for hydrogen evolution reaction. *Int. J. Hydrogen Energy* **2020**, *45*, 10486–10493. [[CrossRef](#)]
22. Singh, K.P.; Shin, C.H.; Lee, H.Y.; Razmjooei, F.; Sinhamahapatra, A.; Kang, J.; Yu, J.S. TiO<sub>2</sub>/ZrO<sub>2</sub> nanoparticle composites for electrochemical hydrogen evolution. *ACS Appl. Nano Mater.* **2020**, *3*, 3634–3645. [[CrossRef](#)]
23. Wang, S.; Yang, P.; Sun, X.; Feng, L.; Jin, C.; Ren, M.; Xing, H.; Shi, J. Fabrication of the flower-like NiCo<sub>2</sub>O<sub>4</sub> @ Ni(OH)<sub>2</sub>/NiOOH composites supported on nickel foam by the green solvent dimethyl sulfoxide with high performance in supercapacitor and hydrogen evolution reaction. *J. Phys. Chem. Solids* **2021**, *159*, 110257. [[CrossRef](#)]
24. Zhang, L.; Zheng, Y.; Wang, J.; Geng, Y.; Zhang, B.; He, J.; Xue, J.; Frauenheim, T.; Li, M. Ni/Mo Bimetallic-Oxide-Derived Heterointerface-Rich Sulfide Nanosheets with Co-Doping for Efficient Alkaline Hydrogen Evolution by Boosting Volmer Reaction. *Small* **2021**, *17*, e2006730. [[CrossRef](#)]
25. Liu, Y.; Zhao, Y.; Yu, Y.; Ahmad, M.; Sun, H. Facile synthesis of single-crystal mesoporous CoNiO<sub>2</sub> nanosheets assembled flowers as anode materials for lithium-ion batteries. *Electrochim. Acta* **2014**, *132*, 404–409. [[CrossRef](#)]
26. Liu, Y.; Zhao, Y.; Yu, Y.; Li, J.; Ahmad, M.; Sun, H. Hierarchical CoNiO<sub>2</sub> structures assembled from mesoporous nanosheets with tunable porosity and their application as lithium-ion battery electrodes. *New J. Chem.* **2014**, *38*, 3084–3091. [[CrossRef](#)]
27. Yeom, H.C.; Moon, D.J.; Lee, K.Y.; Kim, S.W. Formation and characterization of Ni nanofiber catalysts on nickel metallic foam by electrospinning process. *J. Nanosci. Nanotechnol.* **2015**, *15*, 5167–5170. [[CrossRef](#)]
28. Wang, D.; Guo, J.; Hu, D.; Xu, Q.; Zhang, L.G.; Wang, J.D. Co@Co<sub>3</sub>O<sub>4</sub> Prepared in situ from metallic Co as an efficient semiconductor catalyst for photocatalytic water oxidation. *ACS Sustain. Chem. Eng.* **2018**, *6*, 8300–8307. [[CrossRef](#)]
29. Yan, X.; Li, K.; Lyu, L.; Song, F.; He, J.; Niu, D.; Liu, L.; Hu, X.; Chen, X. From water oxidation to reduction: Transformation from Ni<sub>(x)</sub>Co<sub>(3-x)</sub>O<sub>4</sub> nanowires to NiCo/NiCoO<sub>(x)</sub> heterostructures. *ACS Appl. Mater. Interfaces* **2016**, *8*, 3208–3214. [[CrossRef](#)]
30. Xiao, Y.; Zhang, P.; Zhang, X.; Dai, X.; Ma, Y.; Wang, Y.; Jiang, Y.; Liu, M.; Wang, Y. Bimetallic thin film NiCo-NiCoO<sub>2</sub>@NC as a superior bifunctional electrocatalyst for overall water splitting in alkaline media. *J. Mater. Chem. A* **2017**, *5*, 15901–15912. [[CrossRef](#)]
31. Wang, Z.; Zeng, S.; Liu, W.; Wang, X.; Li, Q.; Zhao, Z.; Geng, F. Coupling molecularly ultrathin sheets of NiFe-layered double hydroxide on NiCo<sub>2</sub>O<sub>4</sub> nanowire arrays for highly efficient overall water-splitting activity. *ACS Appl. Mater. Interfaces* **2017**, *9*, 1488–1495. [[CrossRef](#)] [[PubMed](#)]
32. Faid, A.Y.; Barnett, A.O.; Seland, F.; Sunde, S. Ni/NiO nanosheets for alkaline hydrogen evolution reaction: In situ electrochemical-Raman study. *Electrochim. Acta* **2020**, *361*, 137040. [[CrossRef](#)]
33. Wei, B.B.; Wu, J.; Mei, G.; Qi, Z.B.; Hu, W.S.; Wang, Z.C. NiCo<sub>2</sub>O<sub>4</sub> nanowire arrays rich in oxygen deficiencies for hydrogen evolution reaction. *Int. J. Hydrogen Energy* **2019**, *44*, 6612–6617. [[CrossRef](#)]
34. Kong, Q.; Feng, W.; Ma, S.; Sun, F.; Xie, X.; Sun, C. Hydrothermal synthesis of nanoporous NiO rods self-supported on Ni foam as efficient electrocatalysts for hydrogen evolution reaction. *JOM* **2018**, *71*, 621–625. [[CrossRef](#)]
35. Hao, S.; Cao, Q.; Yang, L.; Che, R. Morphology-optimized interconnected Ni<sub>3</sub>S<sub>2</sub> nanosheets coupled with Ni(OH)<sub>2</sub> nanoparticles for enhanced hydrogen evolution reaction. *J. Alloys Compd.* **2020**, *827*, 154163. [[CrossRef](#)]
36. Sung, M.C.; Lee, G.H.; Kim, D.W. CeO<sub>2</sub>/Co(OH)<sub>2</sub> hybrid electrocatalysts for efficient hydrogen and oxygen evolution reaction. *J. Alloys Compd.* **2019**, *800*, 450–455. [[CrossRef](#)]
37. Ullah, N.; Xie, M.; Chen, L.; Yaseen, W.; Zhao, W.; Yang, S.; Xu, Y.; Xie, J. Novel 3D graphene ornamented with CoO nanoparticles as an efficient bifunctional electrocatalyst for oxygen and hydrogen evolution reactions. *Mater. Chem. Phys.* **2021**, *261*, 124237. [[CrossRef](#)]

38. Mohan Kumar, G.; Ilanchezhian, P.; Siva, C.; Madhankumar, A.; Kang, T.W.; Kim, D.Y. Co-Ni based hybrid transition metal oxide nanostructures for cost-effective bi-functional electrocatalytic oxygen and hydrogen evolution reactions. *Int. J. Hydrogen Energy* **2020**, *45*, 391–400. [[CrossRef](#)]
39. Ibupoto, Z.H.; Tahira, A.; Tang, P.; Liu, X.; Morante, J.R.; Fahlman, M.; Arbiol, J.; Vagin, M.; Vomiero, A. MoS<sub>x</sub>@NiO composite nanostructures: An advanced nonprecious catalyst for hydrogen evolution reaction in alkaline media. *Adv. Funct. Mater.* **2019**, *29*, 1807562. [[CrossRef](#)]

**Disclaimer/Publisher's Note:** The statements, opinions and data contained in all publications are solely those of the individual author(s) and contributor(s) and not of MDPI and/or the editor(s). MDPI and/or the editor(s) disclaim responsibility for any injury to people or property resulting from any ideas, methods, instructions or products referred to in the content.